ELSEVIER

Volume 181, Number 2, February 2008

JOURNAL OF SOLID STATE CHEMISTRY

www.elsevier.com/locate/jssc

CONTENTS

Abstracted/indexed in BioEngineering Abstracts, Chemical Abstracts, Coal Abstracts, Current Contents/Physics, Chemical, & Earth Sciences, Engineering Index, Research Alert, SCISEARCH, Science Abstracts, and Science Citation Index. Also covered in the abstract and citation database SCOPUS®. Full text available on ScienceDirect®.

Regular Articles

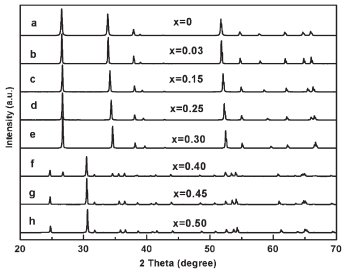

Fe^{3+}–Nb^{5+} co-doped SnO_2 was prepared at 1200 °C by a simple chemical co-precipitation method. The $Sn_{1-2x}Fe_xNb_xO_2$ solid solutions kept cassiterite structure in the range of $0<x\leqslant 0.33$, and their cell parameters decrease with increasing x. While $x=0.40$, a second phase with orthorhombic $FeNbO_4$ structure co-exists with the cassiterite phase, and the second phase becomes dominant while $x\geqslant 0.45$. The magnetic measurements indicated that low doping ratio sample ($x=0.03$) exhibits paramagnetic behavior. A paramagnetic-to-antiferromagnetic phase transition was observed for the samples with higher doping ratio ($x\geqslant 0.15$).

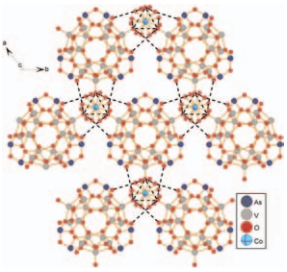

Two novel hydrogen bond-supported supramolecular compounds $[H_2As_6V_{15}O_{42}(H_2O)][Co(H_2O)_6]_2\ldots 2H_2O$ (**1**) and $[H_2As_6V_{15}O_{42}(H_2O)][Ni(H_2O)_6]_2\ldots 2H_2O$ (**2**) have already been synthesized and characterized by X-ray diffraction analyses, they are isostructural and are constructed from arsenic–vanadium clusters and $[Co(H_2O)_6]^{2+}$ or $[Ni(H_2O)_6]^{2+}$ cations, respectively, Each of which exhibits novel 2-D supramolecular architecture.

Regular Articles—Continued

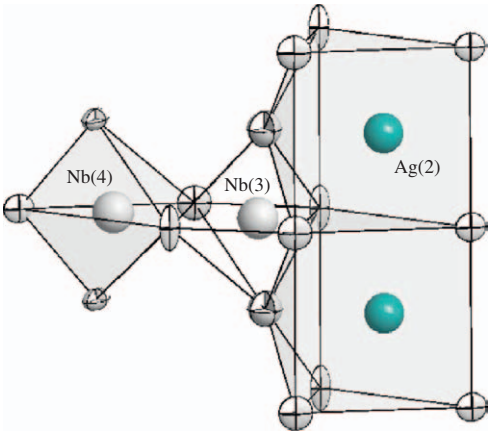

The investigation via conventional solid-state route allows to settle the different compounds of the $AgNbO_3$–Nb_2O_5 system. The structure of a new form of $AgNb_3O_8$ is detailed. It is related to the TTB type network with a specific mixed Ag/Nb occupancy of pentagonal tunnel driving to possible but not observed ordering.

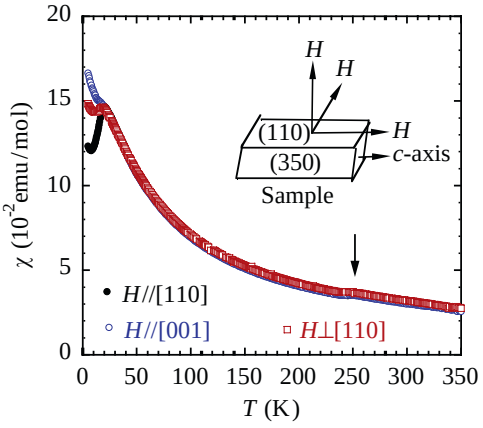

A structural phase transition of the α–β forms occurs at 200–250 K and an antiferromagnetic ordering occurs at ~20 K. A field-induced spin-flop transition shows that spins of Mn^{2+} ions in $Mn_2V_2O_7$ may locate within honeycomb layers.

Preparation and characterization of three-dimensionally ordered macroporous yttria-stabilized zirconia by aqueous organic gel route

J.P. Zhao, Y. Li, W.H. Xin and X. Li

page 239

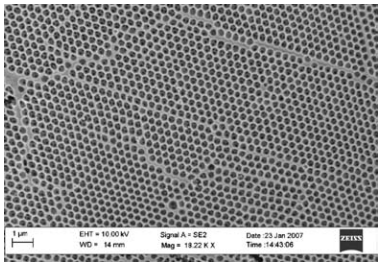

Three-dimensionally ordered macroporous yttria-stabilized zirconia (YSZ) was prepared by aqueous organic gel method through the interstitial spaces between polystyrene spheres assembled on glass substrates. The morphologies of the porous YSZ, the thermal behavior, the phase and chemical composition of polystyrene/YSZ composite were investigated. Ni/YSZ was also prepared and the electrical conductivity was measured.

Studies on the magnetism of cobalt ferrite nanocrystals synthesized by hydrothermal method

Lijun Zhao, Hongjie Zhang, Yan Xing, Shuyan Song, Shiyong Yu, Weidong Shi, Xianmin Guo, Jianhui Yang, Yongqian Lei and Feng Cao

page 245

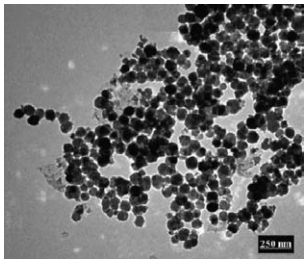

$CoFe_2O_4$ ferrite with a single-domain critical size of 70 nm was fabricated by controlling the hydrothermal reaction conditions carefully, which presents high coercive force (ca. 4.6 kOe) and high squareness ratio (ca. 0.65).

Phase stability and ionic conductivity in substituted $La_2W_2O_9$

D. Marrero-López, J. Peña-Martínez, J.C. Ruiz-Morales and P. Núñez

page 253

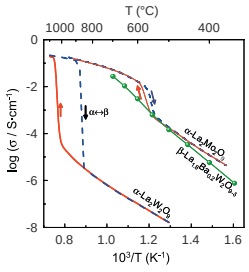

Several substitutions have been tested in order to investigate the stabilisation of the high temperature cubic β-$La_2W_2O_9$ and to obtain new ionic conductors with LAMOX structure without molybdenum composition.

$La_4(Si_{5.2}Ge_{2.8}O_{18})(TeO_3)_4$ and $La_2(Si_6O_{13})(TeO_3)_2$: Intergrowth of the lanthanum(III) tellurite layer with the XO_4 (X = Si/Ge) tetrahedral layer

Fang Kong, Hai-Long Jiang and Jiang-Gao Mao

page 263

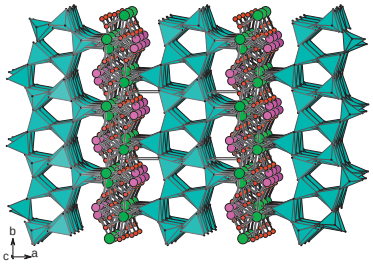

The first lanthanum(III) silicate/germanate tellurites, namely, $La_4[(Si_xGe_{8-x})O_{18}](TeO_3)_4$ ($x = 5.18$) and $La_2(Si_6O_{13})(TeO_3)_2$, have been synthesized and structurally determined by single crystal X-ray diffraction. Both compounds feature complicated 3D network structures composed of the silicate/germanate tetrahedral layers alternating with the $[LaTeO_3]$ layers.

MAS-NMR study of lithium zinc silicate glasses and glass-ceramics with various ZnO content

Madhumita Goswami, Govind P. Kothiyal, Lionel Montagne and Laurent Delevoye

page 269

^{29}Si and ^{31}P MAS-NMR analyses were carried out on multi-component Li_2O–SiO_2–ZnO–Na_2O–P_2O_5–B_2O_3 glasses and glass-ceramics developed for sealing application. Structural data are reported, including phase separation process and quantification of amorphous and crystalline phases.

On the correct spin lattice for the spin-gapped magnetic solid $NH_4CuPO_4 \cdot H_2O$

Hyun-Joo Koo and Myung-Hwan Whangbo

page 276

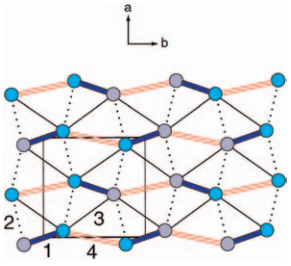

The quantitative mapping analysis based on the present GGA + U calculations indicates that the magnetic properties of $NH_4CuPO_4 \cdot H_2O$ should be described by an AF–F alternating chain model, although an isolated AFM dimer model has been considered to be correct.

Continued

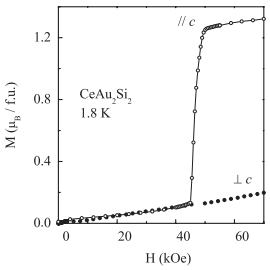

The magnetization versus applied field for $CeAu_2Si_2$ along two crystallographic directions.

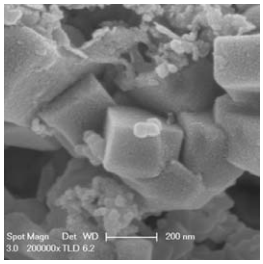

Nanocrystalline lanthanum hexaboride (LaB_6) with mean particle size of 30 nm has been successfully synthesized at 400 °C in an autoclave starting from $NaBH_4$, $LaCl_3$ and metallic magnesium powder. In this case, by using B_2O_3 instead of $NaBH_4$, LaB_6 nanocubes with mean size of ~200 nm were formed at 500 °C. In comparison with previous routes, the present route allows for the formation of nanocrystalline LaB_6 through a simpler process and at a much lower synthesis temperature.

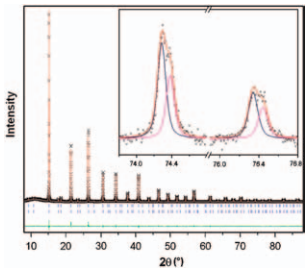

The incompatibility of Sb and Nb in single-phase perovskites is explored for two families of oxides, namely Ba_2EuNbO_6–Ba_2PrSbO_6 and Ba_2NdSbO_6–Ba_2NdNbO_6. Limited solubility of Sb^{5+} in these Nb^{5+} perovskites is observed, irrespective of their precise structure. This is apparently a consequence of competing bonding requirements of the Nb^{5+} and Sb^{5+} cations.

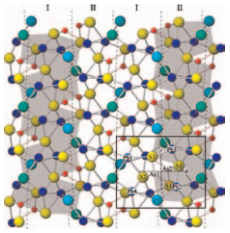

In the crystal structure of mutnovskite at 110 K the two halogens I and Cl are ordered into two specific sites and only slight changes in the coordination environment around Pb atoms occur during the phase transition $Pnma \rightarrow Pnm2_1$ from the RT-structure to the LT-structure. Two kinds of layers alternating along **a** are present in the LT-structure: Layer I contains Cl atoms and [001] columns of Pb1 and Pb4 prisms, layer II contains I atoms and [001] columns of Pb2 and Pb3 prisms.

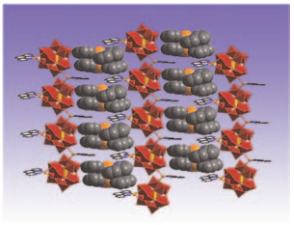

A novel hybrid solid, $\{Ag(phen)_2\}_2\{[Ag(phen)]_2[PMo_{12}O_{40}]\}$ (phen = 1,10-phenanthroline) **1**, is reported. In the structure of **1**, $\{Ag(phen)[PMo_{12}O_{40}]\}^{3-}$ polyanions are connected by $\{Ag(phen)\}^+$ fragments to form a hybrid chain structure. $\{Ag(phen)_2\}^+$ counter-cations are involved in inter-chain π–π stacking to form a three-dimensional supramolecular framework. Luminescent investigation of **1** indicates that **1** displays fascinating orange luminescent property at ambient temperature.

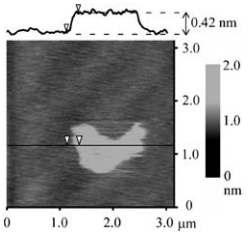

Potassium-intercalated layered niobium sulfide has been synthesized by heating a corresponding layered niobate in a H_2S/N_2 mixture gas. Proton-exchanged layered niobium sulfide has been exfoliated into NbS_2 mono-nanosheet. The NbS_2 mono-nanosheet was restacked with cationic species by an electrostatic self-assembly deposition.

Nanorod γ-Mo_2N.

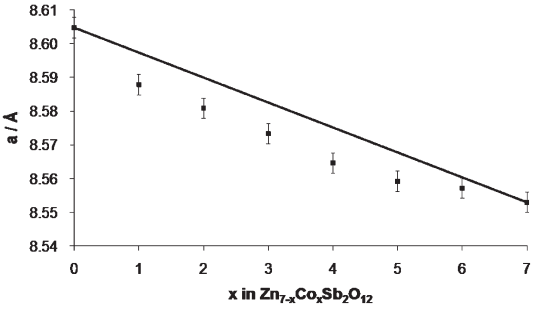

$Zn_7Sb_2O_{12}$ forms a full range of Co-containing α solid solutions, $Zn_{7-x}Co_xSb_2O_{12}$, with an inverse-spinel structure at high temperature. From the Rietveld refinement using ND data, Co occupies both octahedral and tetrahedral sites at intermediate values of x, but an octahedral preference attributed to crystal field stabilisation, causes the lattice parameter plot to deviate negatively from the Vegard's law.

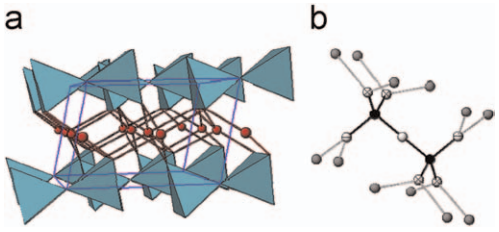

T–O bridging distance and mean T–O distance are linearly correlated to the total atomic valence of the bridging oxygen and the silicon, respectively, and they are a function of the principal quantum number (n) of the valence shell of the atom T.

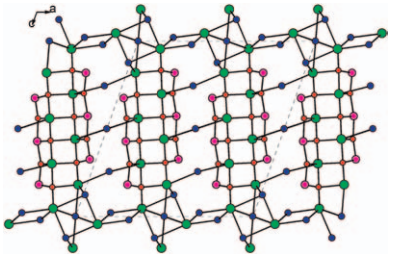

Solid-state reactions of SrO, $SrCl_2$, and SeO_2 or TeO_2 in different molar ratios and under different temperatures lead to two new strontium selenium(IV) or tellurium(IV) oxychlorides with two different types of structures, namely, $Sr_3(SeO_3)(Se_2O_5)Cl_2$ and $Sr_4(Te_3O_8)Cl_4$. Both compounds are wide band-gap semiconductors based on the diffuse reflectance spectra and the electronic band structures.

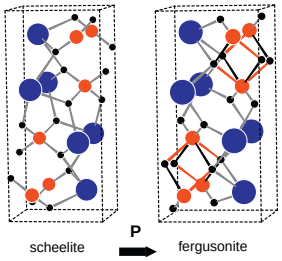

The evolution of the structure of $SrMoO_4$ upon compression was established using synchrotron X-ray diffraction and a diamond-anvil cell. A pressure-induced phase transition was found involving a symmetry decrease from tetragonal to monoclinic. A transition mechanism is proposed and its ferroelastic character is discussed in terms of the Landau theory.

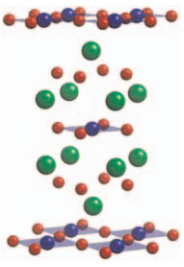

Superconductivity in the electron-doped $(Nd_{1-x}Ce_x)_2Cu_{1-y}O_{4+\delta}$ system is sensitively controlled not only by the Ce^{IV}-for-Nd^{III} substitution level (x) but also by the the Cu-vacancy concentration (y) and the oxygen content (δ) determined by oxygen-partial pressure used for the post-annealing.

Continued

Hydrothermal chemistry of Th(IV) with aromatic dicarboxylates: New framework compounds and *in situ* ligand syntheses

Kate L. Ziegelgruber, Karah E. Knope, Mark Frisch and Christopher L. Cahill

page 373

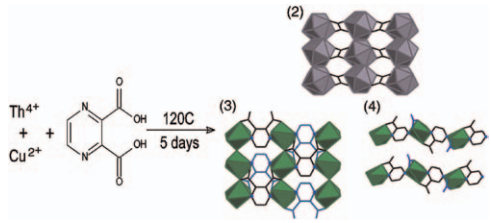

3,5-Pyrazoledicarboxylic and 2,3-pyridinedicarboxylic acid were utilized in synthesizing two novel thorium (IV) coordination polymers. Attempts to synthesize a Th–Cu bimetallic compound with 2,3-pyridinedicarboxylic acid resulted in a triphasic mixture (**2**, **3** and **4**, respectively). The oxalate anion observed in $Th(C_2O_4)_2(H_2O)_2 \cdot 2H_2O$ (**2**) is theorized to result from decarboxylation of 2,3-pyridinedicarboxylic acid as supported by the organic linker, 2-pyrazinecarboxylate, observed in $Cu(C_5H_3N_2O_2)(NO_3)(H_2O)$ (**4**).

Hydrothermal syntheses, structural, Raman, and luminescence studies of $Cm[M(CN)_2]_3 \cdot 3H_2O$ and $Pr[M(CN)_2]_3 \cdot 3H_2O$ (M = Ag, Au) 2. Hetero-bimetallic coordination polymers consisting of trans-plutonium and transition metal elements

Zerihun Assefa, Richard G. Haire and Richard E. Sykora

page 382

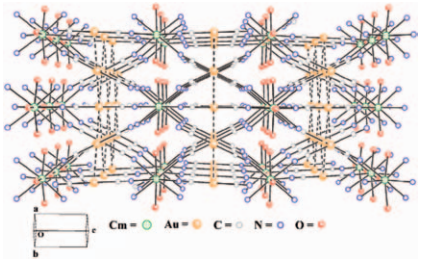

Coordination polymeric compounds between a trans-plutonium element, curium and transition metal ions, gold(I) and silver(I), were prepared using the hydrothermal synthetic procedure. The curium ion and the transition metals are interconnected through cyanide bridging. The Cm ion has a tricapped trigonal prismatic coordination environment with coordination number of nine. Detail photoluminescence studies of the complexes are also reported.